ACS APPLIED MATERIALS & INTERFACES

Research Article

www.acsami.org

Superabsorbent 3D Scaffold Based on Electrospun Nanofibers for Cartilage Tissue Engineering

Weiming Chen,[†,#] Shuai Chen,[‡,#] Yosry Morsi,[§] Hany El-Hamshary,[∥,⊥] Mohamed El-Newhy,[∥,⊥] Cunyi Fan,[*,‡] and Xiumei Mo[*,†]

[†]State Key Laboratory for Modification of Chemical Fibers and Polymer Materials, College of Chemistry, Chemical Engineering and Biotechnology, Donghua University, Shanghai 201620, China

[‡]Department of Orthopaedics, Shanghai Jiao Tong University Affiliated Sixth People's Hospital, 600 Yishan Road, Shanghai 200233, China

[§]Faculty of Engineering and Industrial Sciences, Swinburne University of Technology, Hawthorn, Vic 3122, Australia

[∥]Department of Chemistry, College of Science, King Saud University, Riyadh 11451, Kingdom of Saudi Arabia

[⊥]Department of Chemistry, Faculty of Science, Tanta University, Tanta 31527, Egypt

Supporting Information

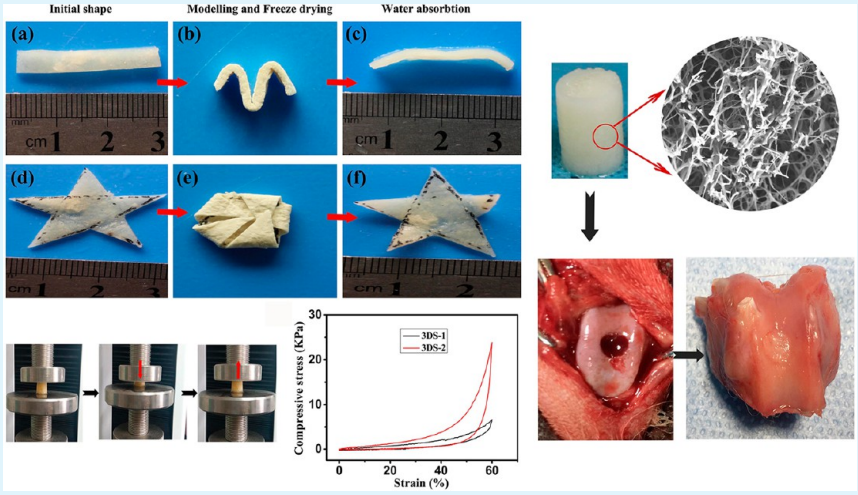

ABSTRACT: Electrospun nanofibers have been used for various biomedical applications. However, electrospinning commonly produces two-dimensional (2D) membranes, which limits the application of nanofibers for the 3D tissue engineering scaffold. In the present study, a porous 3D scaffold (3DS-1) based on electrospun gelatin/PLA nanofibers has been prepared for cartilage tissue regeneration. To further improve the repairing effect of cartilage, a modified scaffold (3DS-2) cross-linked with hyaluronic acid (HA) was also successfully fabricated. The nanofibrous structure, water absorption, and compressive mechanical properties of 3D scaffold were studied. Chondrocytes were cultured on 3D scaffold, and their viability and morphology were examined. 3D scaffolds were also subjected to an in vivo cartilage regeneration study on rabbits using an articular cartilage injury model. The results indicated that 3DS-1 and 3DS-2 exhibited superabsorbent property and excellent cytocompatibility. Both these scaffolds present elastic property in the wet state. An in vivo study showed that 3DS-2 could enhance the repair of cartilage. The present 3D nanofibrous scaffold (3DS-2) would be promising for cartilage tissue engineering application.

KEYWORDS: *3D scaffold, electrospun nanofiber, cartilage tissue engineering, superabsorbent, cross-linking*

1. INTRODUCTION

In recent years, electrospinning nanofibers have gained widespread interest for tissue engineering application. Electrospinning is regarded as a simple approach for creating nanofibrous networks which can mimic the structure of an extracellular matrix (ECM). A variety of tissue engineering scaffolds based on electrospun nanofibers have been developed.[1−3] The advantages of an electrospun nanofiber scaffold are remarkable such as high porosity and high surface-to-volume ratio, which is beneficial for cell communication, cell adhesion, and nutrient transport.[2,4] Tissue engineering provides a potential approach for the regeneration of cartilage, and many

Received: June 7, 2016
Accepted: August 25, 2016
Published: August 25, 2016

DOI: 10.1021/acsami.6b06825
ACS Appl. Mater. Interfaces 2016, 8, 24415−24425

scaffolds based on electrospun nanofibers have been created for cartilage repair.[5] Shin et al. fabricated electrospun poly(DL-lactide-*co*-glycolide) (PLGA) nanofiber and investigated its potential to be used for cartilage reconstruction.[6] Chen et al. modified the surface of electrospun poly(lactic acid) (PLLA) nanofibers with gelatin by plasma treatment, and the results indicated that modified PLA nanofibers could enhance proliferation and differentiation of rabbit articular chondrocytes.[7] Shields et al. created a cartilage scaffold with type collagen II and showed that an electrospun collagen scaffold produced a suitable environment for chondrocyte growth.[8] Various scaffolds have been produced for cartilage tissue engineering by electrospun nanofibers. However, most electrospun nanofibrous scaffolds were not suitable for 3D cartilage regeneration because of the low thickness and small pore size of nanofiber membranes. Fabricating a 3D nanofibrous scaffold rather than the conventional 2D membrane is still a major challenge.[9] Significant efforts have been invested for producing a 3D nanofibrous scaffold. There were several approaches to preparing an electrospinning 3D nanofibrous scaffold, such as multilayering electropinning,[9−11] liquid-assisted collection,[12,13] template-assisted collection,[14,15] adding porogen,[16] self-assembly,[17−19] and postprocessing,[20] etc. Each technology has different advantages, but the disadvantages and limitations also existed. Multilayering electropinning and liquid-assisted collection were time-consuming processes; template-assisted collection generally needs a specific collector or complex technique; porogen such as salt needs to be washed away; self-assembly may require a specific condition (e.g., the solution viscosity, collector, electrostatic field) for preparing the 3D scaffold.[9] Exploring a novel method to fabricate 3D nanofibrous scaffolds with desired shape, pore size, and mechanical property is necessary for cartilage tissue engineering.

To fabricate 3D nanofibrous and mechanically stable scaffolds, novel and feasible approaches were presented by some research groups. Lavielle et al.[21] and Wittmer et al.[22] combined electrosprayed microparticles with electrospinning nanofibers to fabricate a composited 3D scaffold, which presents hierarchical porous structure. However, the concern was that PEG particles in the composited scaffold would dissolve in aqueous solution, and PLA particles which were smaller than 10 μm in diameter might enter into cells by phagocytosis.[23] Recently, Ding,[24,25] Greiner,[26] and Fong[27] have, respectively, reported 3D nanofiber-assembled cellular aerogels or scaffolds by combining electrospinning and freeze-drying techniques. The methods provided by them were similar: nanofiber membranes were first cut into small pieces, and then the pieces of nanofibers were frozen and freeze-dried to obtain a 3D nanofibrous structure. This process of fabricating a scaffold reported by them was efficient and had some advantages: (1) the scaffold was assembled by nanofibers with cellular structure, which might be favorable for cell proliferation and infiltration; (2) the scaffold presented good reversible compressibility, and proper and stable mechanics was important for the tissue engineering scaffold; (3) desire and diverse shapes could be obtained; (4) the method was relatively easy, and any complex devices were not required. Ding et al. fabricated nanofiber-assembled aerogels, which exhibited superelasticity and multifunctionality,[25] but the polyacrylonitrile (PAN) was not a biocompatible material, which was not suitable for tissue engineering. Greiner et al. produced high porous polymer sponges with short electrospun fibers, which was an attempt to mimic the design principle of nature sponges.[26] However, the sponge was made of poly(MA-*co*-MMA-*co*-MABP), which was nondegradable and had limitations for tissue engineering application.[27] Biocompatible materials would be a better choice for tissue engineering scaffold. Fong et al. reported an electrospun PCL 3D nanofibrous scaffold for bone tissue engineering, which possessed interconnected and hierarchically structured pores. The PCL scaffold was prepared by thermally induced self-agglomeration followed by freeze-drying and could promote BMP-2 induced osteogenic differentiation of mBMSCs.[27] However, there also existed some problems on this scaffold: (1) for preparing short nanofibers, electrospun PCL mats were put in liquid nitrogen and grinded in a mortar, which is not a convenient operation and suitable for mass production; (2) this scaffold was prepared by synthetic (PCL) that would exhibit hydrophobic property and lack cell recognition.[4] It is desirable to fabricate a scaffold with biocompatible and biodegradable materials. Composite polymer combined by natural and synthetic polymers was a commonly used material for the tissue engineering scaffold, which could possess a bioactive surface and mechanical properties.[4] In our previous study, a 3D nanofibrous scaffold made of gelatin and PLA was prepared for tissue engineering, which presented superabsorbent properties.[28] To cross-link gelatin and obtain stable bonded elastic fibrous networks, glutaraldehyde was used as cross-linking agent. However, the glutaraldehyde is toxic, and it may release into the host due to the biodegradation of scaffold.[29]

Herein, we reported a 3D scaffold based on electrospun gelatin/PLA nanofibers, which was fabricated by a convenient method. For the first time, we developed a process to cross-link gelatin/PLA nanofibrous scaffold (3DS-1), which was heated by high temperature and followed by water treatment (heat and water). The resulting scaffold (3DS-1) exhibits hierarchical cellular structure and superabsorbent property. In the wet state, 3DS-1 could bear a compressive strain as high as 60% and recovers its original shape after the stress released. An in vitro study showed that 3DS-1 could enhance the growth and proliferation of chondrocytes. In order to investigate the cartilage repair capacity of 3DS-1 in vivo, cartilage defects were created in the rabbit. The in vivo study showed that the cartilage repair capacity of 3DS-1 was limited. To further improve the repair and regeneration capacity, 3D scaffold was modified by hyaluronic acid (HA), which was found natively in cartilage tissue. The modified scaffold (3DS-2) also exhibited cellular structure and superabsorbent property. Moreover, 3DS-2 presented greater compressive strength than 3DS-1. An in vivo study indicated that 3DS-2 could enhance repair cartilage defects in rabbit. 3DS-2 might be promising for cartilage tissue engineering application.

2. MATERIALS AND METHODS

2.1. Materials. Type A gelatin was purchased from MP Biomedicals, LLC. PLLA was a gift provided by Medprin Regenerative Medical Technologies (Guangzhou, China). Hyaluronic acid (sodium salt) was purchased from Bloomage Freda Biopharm Co., Ltd. The DMEM/F12 (1:1, Hyclone), fetal bovine serum (FBS, Gibico), and trypsin (hyclone) were purchased from Yuanzhi Biotechnology Co., Ltd. Live&Dead viability assay kit was purchased from KeyGEN BioTECH Corp., Ltd. All other chemicals were of analytical grades and were used without further purification.

2.2. Preparation of Electrospun Gelatin/PLA Nanofibers. The preparation of the electrospun gelatin/PLA nanofibers had been described in our previous study.[28] Gelatin and PLA were all dissolved in 1,1,1,3,3,3-hexafluoro-2-propanol (HFIP), and the total concen-

DOI: 10.1021/acsami.6b06825
ACS Appl. Mater. Interfaces 2016, 8, 24415−24425

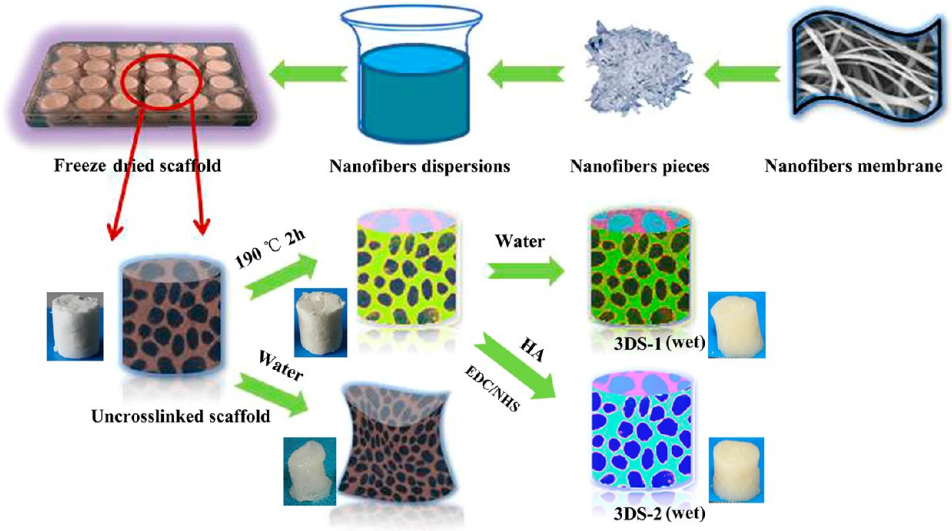

Figure 1. Schematic illustration for 3D scaffold preparation.

tration of polymer was 11% (W/V). The mass ratio of gelatin and PLA was 5:1. The applied voltage, the electrospinning distance, and the flow rate were controlled at 15 kV, 10 cm, and 5 mL/h, respectively. The obtained gelatin/PLA nanofiber membranes were placed in vacuum for storage.

2.3. Preparation of 3DS-1 and 3DS-2. First, heat-treated scaffold was prepared by following three steps: (1) electrospun gelatin/PLA nanofiber membranes were cut into small pieces (1 cm × 1 cm); (2) the pieces of nanofiber membranes were dispersed in *tert*-butanol by homogenizing with IKA T18 homogenizer; the revolving speed was 10 000 rpm, and the stirring time was 30 min; (3) the uniform nanofiber dispersions were poured into the cell culture plate, frozen in −20 °C for 0.5 h and freeze-dried for 24 h, and then the dried 3D scaffold was heated at 190 °C for 2 h in air. Second, 3DS-1 and 3DS-2 were prepared with heat-treated scaffolds by different treatments, respectively. For preparing 3DS-1, heat-treated scaffold was immersed in water for 2 h, and then the wet scaffold was frozen in −80 °C for 2 h and freeze-dried for 48 h. For preparing 3DS-2, heat-treated scaffold was cross-linked with 50 mL of solution containing 1% HA, 30 mM *N*-[3-(dimethylamino)propyl]-*N*′-ethylcarbodiimide hydrochloride (EDC), 8 mM *N*-hydroxysuccinimide (NHS), and 50 mM MES buffer for 2 h.[30] The scaffold was subsequently washed with distilled water to remove free HA and salt, frozen in −80 °C for 2 h, and then freeze-dried for 48 h.

2.4. Characterization. *2.4.1. Fourier Transform Infrared Spectroscopy.* Attenuated total reflection Fourier transform infrared spectroscopy (ATR-FTIR) of scaffolds were obtained using a Nicolet-670 FTIR spectrometer. All spectra were recorded at a wavelength range of 1000 to 4000 cm^{-1}.

2.4.2. Morphology and Density of the 3D Scaffold. The surface morphology of the scaffold was observed by scanning electron microscopy (SEM, Hitachi TM-1000, Japan) at an accelerating voltage of 15 kV.

The densities (ρ) of the 3D scaffold were calculated using the following equation[26]

$$\rho = m/v = (4m)/(\pi d^2 h) \quad (1)$$

Here, m, v, d, and h stand for mass, volume, diameter, and height of the scaffold, respectively.

2.4.3. Water Absorption Capacity of the 3D Scaffold. Water absorption capacity tests were conducted following the reported method.[31] Each dry weight of scaffolds was weighted and recorded (w_d). The scaffold was put into distilled water and removed after 2.5, 10, 30, 60, and 120 min. The superficial water of scaffold was gently blotted on a filter paper. Then the wet weight of 3D scaffolds was weighted and recorded (w_w). The water absorption capacity (w) of the 3D scaffolds was calculated using the following equations

$$w = (w_w - w_d)/w_d \times 100\% \quad (2)$$

w_d and w_w were the weight of dry and wet 3D scaffolds, respectively.

2.4.4. Compressive Mechanical Properties of the 3D Scaffold. Compressive mechanical properties of the 3D scaffold were carried out by compression testing machine with a 200 N loaded sensor. Six samples with diameters of 13 mm and height of 14 mm were used for mechanical property study. The first four samples were un-cross-linked scaffold (un-cross-link), scaffold heated at 120 °C for 2 h (120 °C 2 h), 160 °C for 2 h (160 °C 2 h), and 190 °C for 2 h (190 °C 2 h) in air, respectively. The other samples were 3DS-1 and 3DS-2. The compression strain−stress curves of 3DS-1 and 3DS-2 in the wet state with compression strain (ε = 60%) were measured at a strain rate of 10 mm/min.

2.4.5. Cell Viability in the 3D Scaffold. Rat chondrocytes were cultured in DMEM/F12 (1:1) which contains 10% FBS, 100 μg/mL of streptomycin, and 100 U/mL of penicillin. Cells were incubated at 37 °C in a humidified atmosphere containing 5% CO_2. Before cell seeding, the scaffold was immersed in 75% ethanol for about 3 h for sterilization. 200 μL of cell suspension with a cell number of 2×10^4 was seeded on 3DS-1 and 3DS-2. The viability of encapsulated cells was determined using Live & Dead cell viability assays after 3 and 7 days of culture.

For cell morphology study, cells were seeded and cultured on scaffolds for 3 and 7 days. The morphology of cells was observed by SEM. The cell-seeded scaffolds were fixed with 4% paraformaldehyde for 1 h at 4 °C, followed by dehydration with gradient ethanol solution. Then the ethanol in the scaffold was replaced by *tert*-butanol, and the scaffolds were freeze dried at −60 °C for 24 h in vacuum. Afterward, the samples were gold sputtered and observed by SEM at the accelerating voltage of 15 kV.

2.4.6. Animal Implantation, Histological Evaluation, and Immunohistochemical Staining Evaluation. All of the animals were obtained from Shanghai Jiao Tong University and treated according to the standard guidelines approved by Shanghai Jiao Tong University Ethics Committee. Healthy male New Zealand white rabbits weighing 2.5−3 kg were used in this study. An osteochondral defect of 3 mm diameter and 4 mm depth was created in the trochlear groove of the right leg using trephine bur. The rabbits were randomly divided into three groups: the 3DS-1 and 3DS-2 group, defects were implanted with scaffolds; control group, defects were untreated. The rabbits were sacrificed at 12 weeks after surgery.

The harvested histological specimens were fixed in 4% paraformaldehyde for 1 week, decalcified in 10% ethylenediaminetetraacetate

DOI: 10.1021/acsami.6b06825
ACS Appl. Mater. Interfaces 2016, 8, 24415−24425

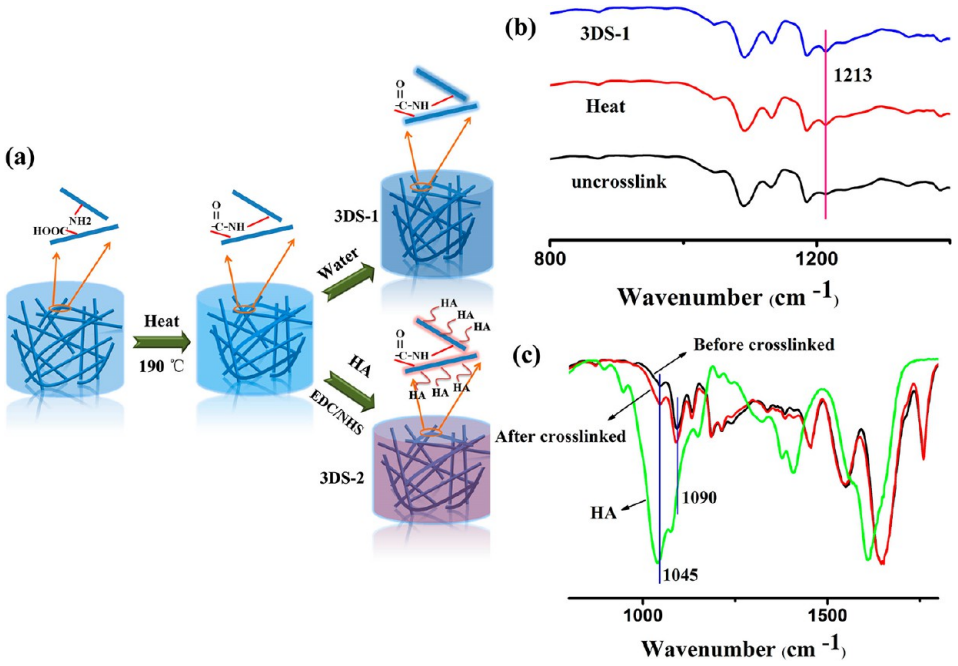

Figure 2. Cross-linking of 3D scaffold and ATR-FTIR analysis. (a) Schematic showing the cross-linking steps. (b) ATR-FTIR spectra of un-cross-linked sample, heat-treated sample, and 3DS-1. (c) ATR-FTIR spectra of HA and 3DS-2 (before and after cross-linked with HA in EDC/NHS solution).

dihydrate (EDTA) solution for 3 weeks, embedded in paraffin, cut into sections 7 μm thick, then stained with hematoxylin and eosin (HE) for morphological evaluation and stained with Safranin O and fast green for glycosaminoglycan (GAG) distribution. Immunohistochemical staining of repaired cartilage was also performed to detect type collagen II and aggrecan deposition. Histological and immunohistochemical staining observation was examined using a light microscope.[32]

2.4.7. Statistical Analysis. All the data were conducted at least in triplicate. Statistical analysis was performed by one-way ANOVA using Origin 8.0. The criteria for statistical significance were $*p < 0.05$.

3. RESULTS AND DISCUSSION

3.1. Preparation of 3D Scaffolds. The schematic of 3D scaffold fabrication was illustrated in Figure 1. The preparation process could be generally divided into three steps: (1) electrospinning; (2) freeze-drying; (3) cross-linking. The fabrication approach was convenient and effective, which was suitable for mass production.

Cross-linking of the scaffold is necessary and important to form a stable morphology and interconnected networks. To retain the original gelatin nanofiber morphology, chemical agents were used for cross-linking.[29,33] Glutaraldehyde or EDC/NHS was a commonly used cross-linking agent for obtaining a stable electrospun gelatin nanofiber. In this study, glutaraldehyde was rejected due to its toxicity. EDC was a relatively low cytotoxic compound; however, un-cross-linked scaffold would collapse after being immersed in water or EDC/NHS solution because gelatin would dissolve in water. In our study, it was found that heat treatment (190 °C) could retain the stability of the scaffold. When the heat-treated scaffold was immersed in water or EDC/NHS solution, it could be observed that the shape of the scaffold was kept as shown in Figure 1. That is because physical treatment such as dehydration could cross-link gelatin and make gelatin insoluble.[34] Scaffolds cross-linked by heat with different temperature were also prepared, which could be seen in the Supporting Information (Figure S1). The scaffolds which were heated at 120 or 160 °C would be out-of-shape when they were immersed in water. However, when the scaffold which was heated at 190 °C was put into water, no deformation was observed. It indicated that heat treatment at 190 °C was effective to the cross-link scaffold. The mechanical property of the heat-treated scaffold was poor, and cross-linking the heat-treated scaffold was also necessary to obtain a scaffold with proper mechanics. Water or EDC/NHS treatment was an effective process to cross-link the heat-treated scaffold. When the heat-treated scaffold absorbed water, the nanofibers would stick together, which lead to an enhanced mechanical property of the scaffold. When the heat-treated scaffold was cross-linked with HA in EDC/NHS solution, more cross-linking sites could be formed, and the compressive strength of the scaffold was also enhanced. The wet 3DS-1 and 3DS-2 were prepared as shown in Figure 1. In addition, cross-linking could prolong the degradation time of the scaffold (Figure S2, Supporting Information). Both 3DS-1 and 3DS-2 present a slow rate of degradation in vitro, and the un-cross-linked scaffold only retained about 20% mass after one month of degradation.

3.2. ATR-FTIR. Figure 2a showed the schematic diagram for a cross-linkng 3D scaffold. Heat treatment could decrease the number of free acidic and basic residues on gelatin and make gelatin insoluble.[35] Interchain cross-linking and amide formation could be formed on gelatin by dehydration.[34,35] The absorption intensity peak at 1213 cm^{-1} assigned to the C−N stretching vibration band was weak and became more intense after heat treatment and heat and water treatment (Figure 2b). As shown in Figure 2c, for pure HA, the peak at 1045 cm^{-1} was attributed to C−O−C strethching in HA. The peak at 1090 cm^{-1} was assigned to the C−O stretching. A slight increasing of absorption intensity peak at 1045 and 1090 cm^{-1} in the spectra of cross-linked scaffold could be observed. EDC could react with rich carboxyl groups in HA to form an activated intermediate acid anhydride, which might react with the

DOI: 10.1021/acsami.6b06825
ACS Appl. Mater. Interfaces 2016, 8, 24415−24425

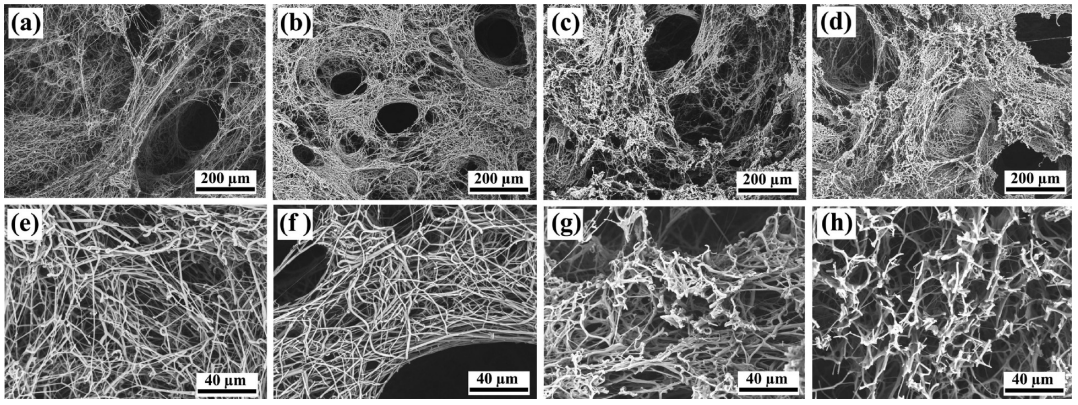

Figure 3. SEM images of 3D scaffolds. Un-cross-linked sample (a, e), heat-treated sample (b, f), 3DS-1 (c, g), and 3DS-2 (d, h).

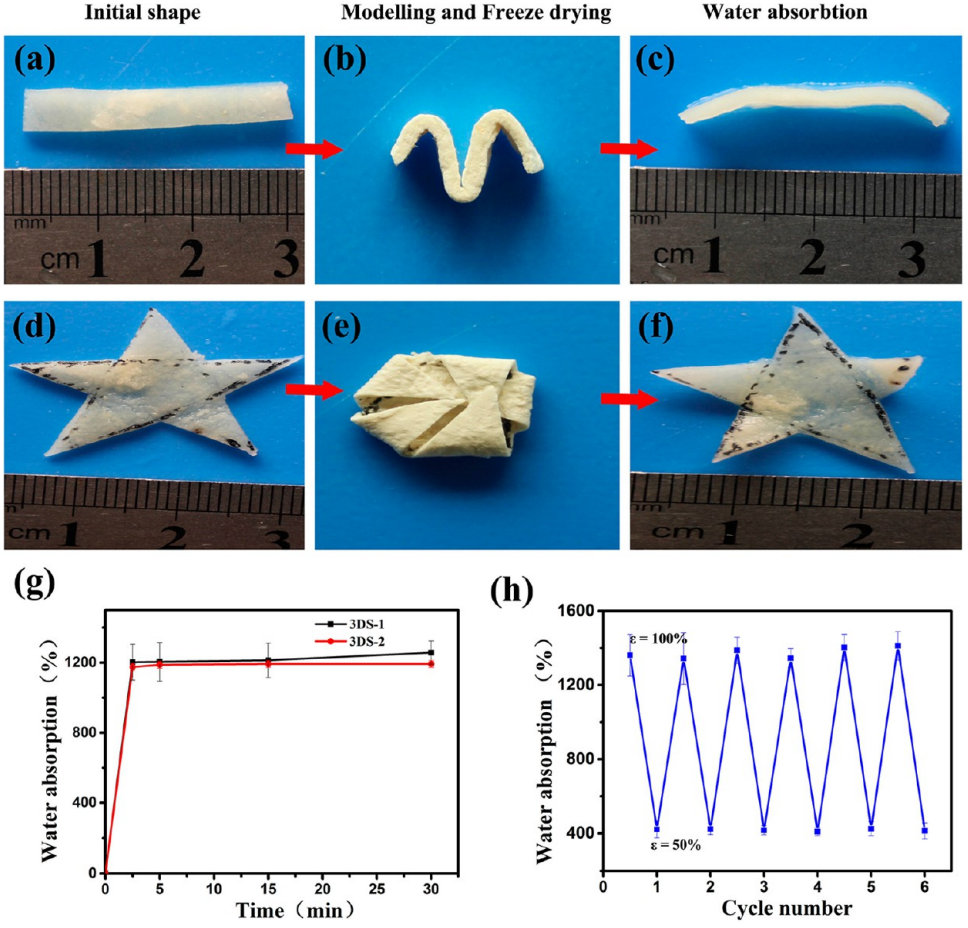

Figure 4. Water absorption property. Photographs showing the scaffold shape recovery after water absorption (3DS-2). (a), (b), and (c) showed rectangular scaffold; (d), (e), and (f) showed quinquangular scaffold. (g) Water absorption rate of the 3DS-1 and 3DS-2. (h) Reversibility of water absorption (3DS-1).

amino group of gelatin to form an amide linkage.[36] However, no obvious new absorption peak was observed in the spectra of 3DS-2 because the absorption peaks assigned to the newly formed function group highly overlap those of the amide group and ester group in gelatin and HA.[36,37]

3.3. Morphology and Density of 3D Scaffolds. Figure 3 showed the SEM images of different 3D scaffolds. It was clearly observed that the scaffolds were constituted of electrospun nanofibers. Various shapes of pores were randomly distributed in the scaffolds. There was no significant difference between Figure 3a and Figure 3b, indicating the morphology of gelatin/PLA nanofibers which had high content of gelatin (83.3%) was not damaged by heat treatment. However, the nanofiber morphology in Figure 3c was different from that in Figure 3a and Figure 3b, and nanofibers seemed to stick together. The reason might be that electrospun gelatin/PLA nanofibers exhibited swelling behavior after water absorption. The nanofiber morphology in 3DS-2 modified by HA (Figure 3d) seemed similar to those in 3DS-1. All scaffolds (Figure 3e, Figure 3f, Figure 3g, and Figure 3h) presented fibrous structure, which was similar to that in natural ECM. Moreover, it would be beneficial for nutrition supply and cell migration. The

DOI: 10.1021/acsami.6b06825
ACS Appl. Mater. Interfaces 2016, 8, 24415−24425

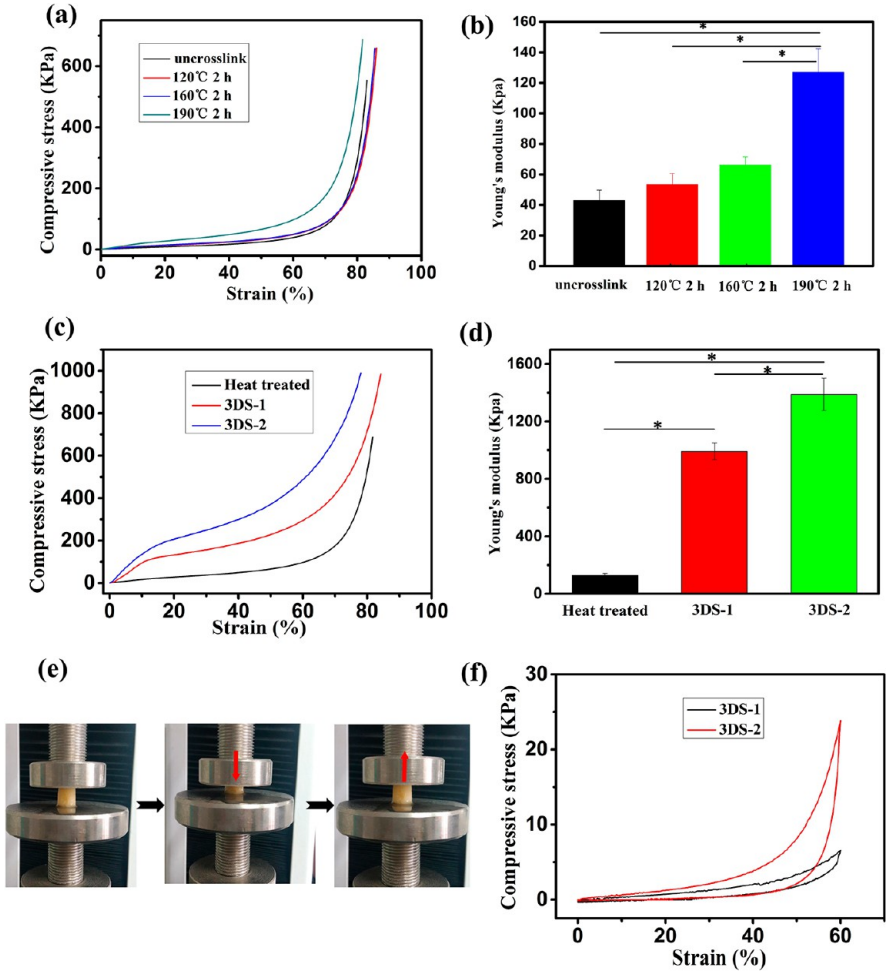

Figure 5. Compressive mechanical properties of different 3D scaffolds. Compressive stress−strain curves (a) and Young's modulus (b) of the scaffold cross-linked at different temperature. Compressive stress−strain curves (c) and Young's modulus (d) of the heat-treated sample, 3DS-1, and 3DS-2. (e) Photographs of the 3DS-2 under a compressing and releasing cycle. (f) Compressive stress−strain curves of the 3DS-1 and 3DS-2 under compressing and releasing cycles (ε = 60%). The samples in (a), (b), (c), and (d) were tested in the dry state, and samples in (e) and (f) were tested in the wet state.

densities of 3DS-1 and 3DS-2 were 94.8 and 103 mg/cm^{-3}, respectively. The density of 3DS-2 was higher than 3DS-1, and the reason might be that HA was added in the scaffold after being cross-linked.

3.4. Water Absorption Capacity. Wettability of biomaterials was one of the most important factors for cell growth, and the hydrophilic scaffold was suitable for cell adhesion.[38] In addition, higher water absorption of the scaffold would benefit cartilage regeneration because water content in cartilage was important for maintaining the resiliency and lubrication of joints.[39] In this study, water absorption property of the scaffold was detected as shown in Figure 4, which presented excellent absorbent property. 3DS-2 was fabricated into a rectangular shape (Figure 4a), and after absorbed water, the wet scaffold showed elastic property and could be folded into "M" shape; the scaffold could keep "M" shape (Figure 4b) by freeze-drying, and the M-shaped scaffold would be almost recovery rectangular shape (Figure 4c) after being immersed in water for 30 min. 3DS-2 was also fabricated into pentacle shape (Figure 4d) and absorbed water, and it was folded into a new model (Figure 4e) and freeze-dried. The folding scaffold could recover pentacle shape (Figure 4f) after absorbing water again. 3DS-1 and 3DS-2 exhibited similar water absorption behavior which was shown in Figure 4g, and both these scaffolds could achieve the maximum water absorption (1300%) in less than 5 min as soon as they came in contact with the water. Moreover, as shown in Figure 4h, by compressing the 3DS-1 with compressive strain of 50%, most absorbed water would be removed, and after the compressive force was released, the scaffold would absorb water and recover its original shape again when immersed in water. The above process was as a cycle, and the scaffold still retained its water absorption capacity after six cycles were repeated.

The excellent absorbent property of the 3D scaffold would be attributed to the hydrophilic property of gelatin and cellular pores of scaffold. The interconnected and porous structure was a beneficial scaffold for absorbing and retaining water. The scaffold could "remember" its original shape after absorbing water, and the reason was that water could infiltrate into the scaffold rapidly and force the folded zone open. The water absorption behavior of the scaffold would be beneficial for biomedical applications; for example, the shape of the cartilage defect might vary, and the scaffold could be fabricated into the needed shape as damaged tissue and could be folded into a small piece which was convenient to implant into the body.

DOI: 10.1021/acsami.6b06825
ACS Appl. Mater. Interfaces 2016, 8, 24415−24425

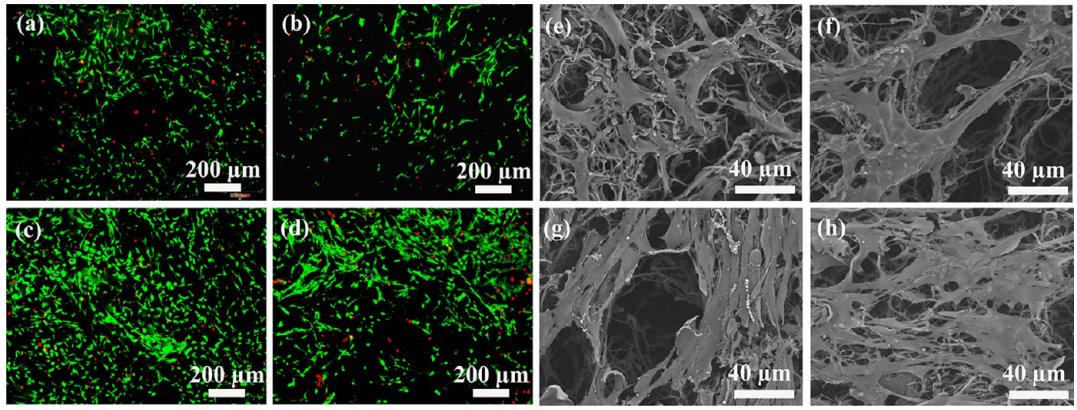

Figure 6. Cell viability assays and cell morphology on scaffolds. Fluorescence micrographs of chondrocytes seeded on 3DS-1 (a and c) and 3DS-2 (b and d) for 3 days (a and b) and 7days (c and d). Live and dead cells dyed green and red, respectively. SEM images of chondrocytes cultured on 3DS-1 (e and g) and 3DS-2 (f and h) for 3 days (e and f) and 7 days (g and h).

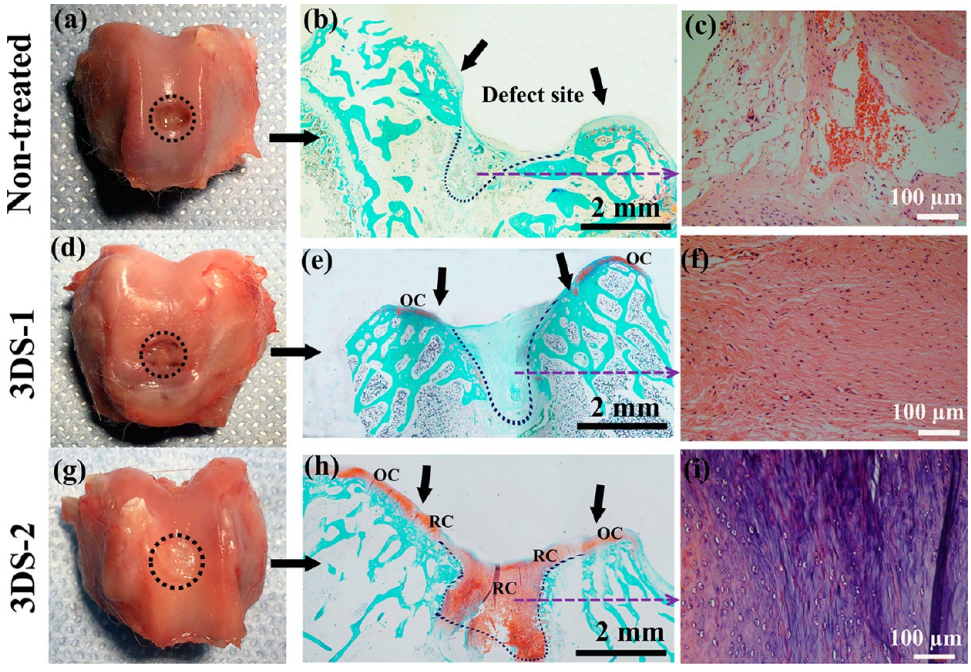

Figure 7. Macroscopic images (a, d, and g) of the cartilage joints from three groups at 12 weeks after surgery. Histological analysis of cartilage defect area from three groups at 12 weeks after surgery, stained with Safranin O-fast green (b, e, and h) and H&E (c, f, and i). Arrows and dotted lines indicated the defect sites. OC: original cartilage tissue. RC: repaired cartilage tissue.

Then the deformed scaffold would absorb joint fluid and fill the damaged tissue.

3.5. Compressive Mechanical Properties of 3D Scaffolds. To investigate the effect of heating temperature on the compressive mechanical property, scaffolds were heated in air at 120 °C, 160 °C, and 190 °C for 2 h, respectively. From stress−strain curves in Figure 5a, it could be observed that the scaffold which was heated at 190 °C showed the highest compressive strength than 120 °C, 160 °C, and un-cross-linked sample. As shown in Figure 5b, the Young's modulus of un-cross-linked, 120 °C, 160 °C, and 190 °C samples was 42.9 KPa, 53.6 KPa, 66.3 KPa, and 127.1 KPa, respectively. The Young's modulus was increased with the increase of heating temperature. High temperature could cross-link gelatin by dehydration, which increased the compressive strength of the scaffold. Comparing the compressive stress−strain curve of the heat-treated sample and 3DS-1 (Figure 5c), 3DS-1 exhibited higher strength. The Young's modulus of 3DS-1 was 992.2 KPa (Figure 5d), which was significantly higher than that of the heat-treated sample. The results indicated that heat and water treatment were an effective procedure for the cross-linking scaffold. The reason might be that nanofibers could stick together after absorbing water, as shown in the SEM images (Figure 3c and Figure 3g). Moreover, the Young's modulus of 3DS-2 was 1389 KPa (Figure 5d), which showed a higher mechanical strength compared to 3DS-1. The results indicated that a scaffold cross-linked with HA could enhance its compressive strength. That might be the reason that 3DS-2 possessed more cross-linked sites and higher density.

3DS-1 and 3DS-2 also exhibited elastic property in the wet state. These two scaffolds could support 60% compressive strain and recover its initial shape after the compressing force was released (Figure 5e). Figure 5f showed the compressive stress−strain curves of the 3DS-1 and 3DS-2 with 60% strain,

DOI: 10.1021/acsami.6b06825
ACS Appl. Mater. Interfaces 2016, 8, 24415−24425

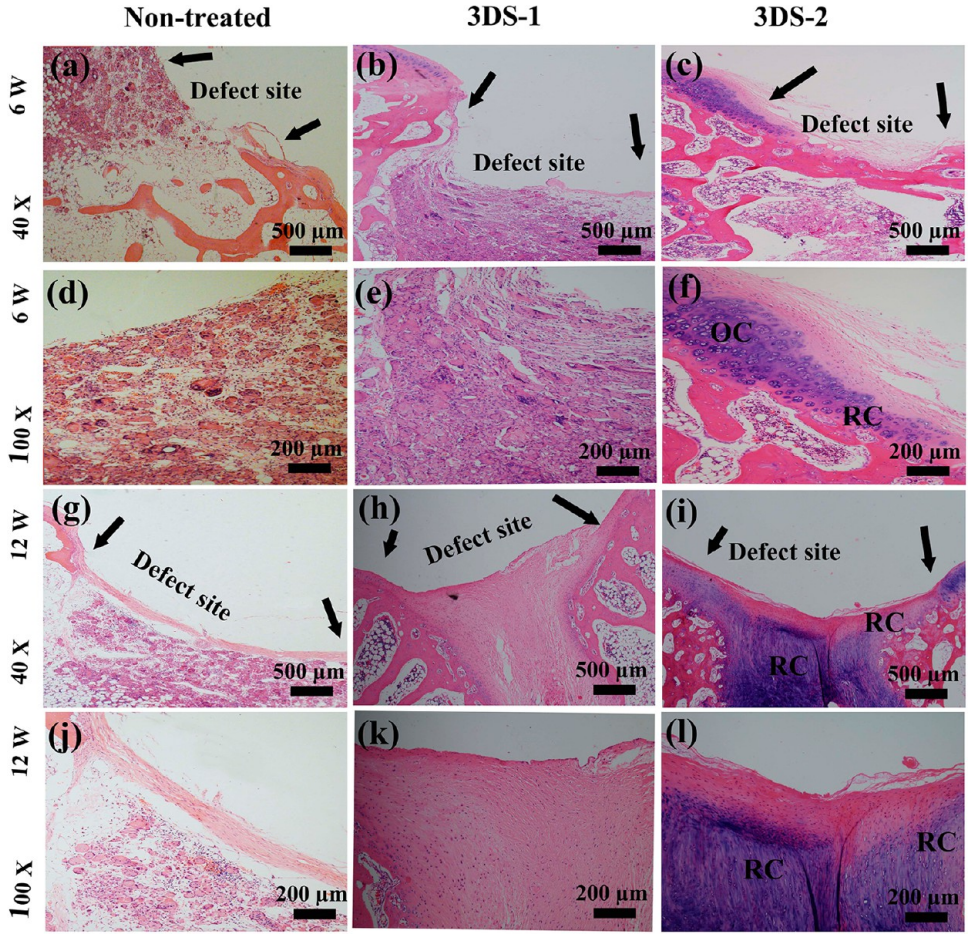

Figure 8. Histological analysis of cartilage defect area from three groups at 6 weeks (a–f) and 12 weeks (g–l) after surgery, stained with H&E. The defect was marked with black arrows in images (a–c, g–i). OC: original cartilage tissue. RC: repaired cartilage tissue.

which all showed a highly nonlinear and closed hysteresis. It was clearly observed that the compressive stress (ε = 60%) of 3DS-2 was significantly higher than that of 3DS-1, which were 23.8 and 6.5 KPa, repectively. During the loading process, there were two states that could be observed, a linear elastic regime at ε < 40% and a sharp stress-increasing regime at ε > 40%.[24] After absorbing water, the water could be removed by compressing the scaffold. When the compressive force was released, the scaffold would absorb the surrounding water due to the excellent water absorption capacity. That might be the reason for the elastic property of the wet scaffold.

3.6. Cell Viability and Cell Morphology on the 3D Scaffold. In order to investigate the cell viability of the 3D scaffold, chondrocytes were cultured on 3DS-1 and 3S-2 for 3 days and 7 days. The cell viability was tested by live and dead assay, which could be found in Figure 6a, Figure 6b, Figure 6c, and Figure 6d. It could be found that live cells (green) grew much more than dead cells (red). After 7 days of culture, live cells on the 3D scaffold linked closely, and only a few dead cells could be observed (Figure 6b and Figure 6d). Cells seeded on 3DS-1 and 3DS-2 presented similar cell viability. The results indicated that the scaffold was noncytotoxic, and cells were able to adhere and proliferate on it. Moreover, this also proved that the cytocompatibility of gelatin and PLA was not destroyed by cross-linking with high temperature. This suggested that both 3DS-1 and 3DS-2 might be suitable for cartilage regeneration.

Cell adhesion and proliferation property of scaffold were evaluated by SEM (Figure 6e, Figure 6f, Figure 6g, and Figure 6h). Chondrocytes were also cultured on 3DS-1 and 3DS-2 for 3 days and 7 days. Cells cultured on these two scaffolds all exhibited good morphology. Cells were able to adhere on the surface of the 3D scaffold and proliferated along the nanofibers. Cells had almost contacted each other and formed a cell sheet (Figure 6g and Figure 6h). The results of cell morphology and cell viability all suggested that the 3DS-1 and 3DS-2 possessed excellent biocompatibility.

3.7. Histological and Immunohistochemical Evaluation. After 12 weeks of implantation, gross appearance revealed that the defect in the nontreated group was not filled, whereas filling of the defect was observed in the 3DS-1 and 3DS-2 group (Figure 7a, Figure 7d, and Figure 7g). In the nontreated group, an obvious defect still existed, and an obvious boundary between the defect and normal tissue could be observed. The nontreated samples stained with Safranin O-fast green (Figure 7b) showed that the defects were not filled overall. Figure 7c showed that the defects were only covered with loose fibrous tissue. However, the defect in 3DS-1 became smaller (Figure 7d) and was filled with dense fibrous tissue (Figure 7e and Figure 7f). Compared with the nontreated group and the 3DS-1 group, the 3DS-2 group exhibited the best cartilaginous regeneration. The defect in the 3DS-2 group was filled with uniform cartilage-like tissue with a flat surface and the defect (Figure 7g). The regenerated cartilage tissue (red color) was

DOI: 10.1021/acsami.6b06825
ACS Appl. Mater. Interfaces 2016, 8, 24415–24425

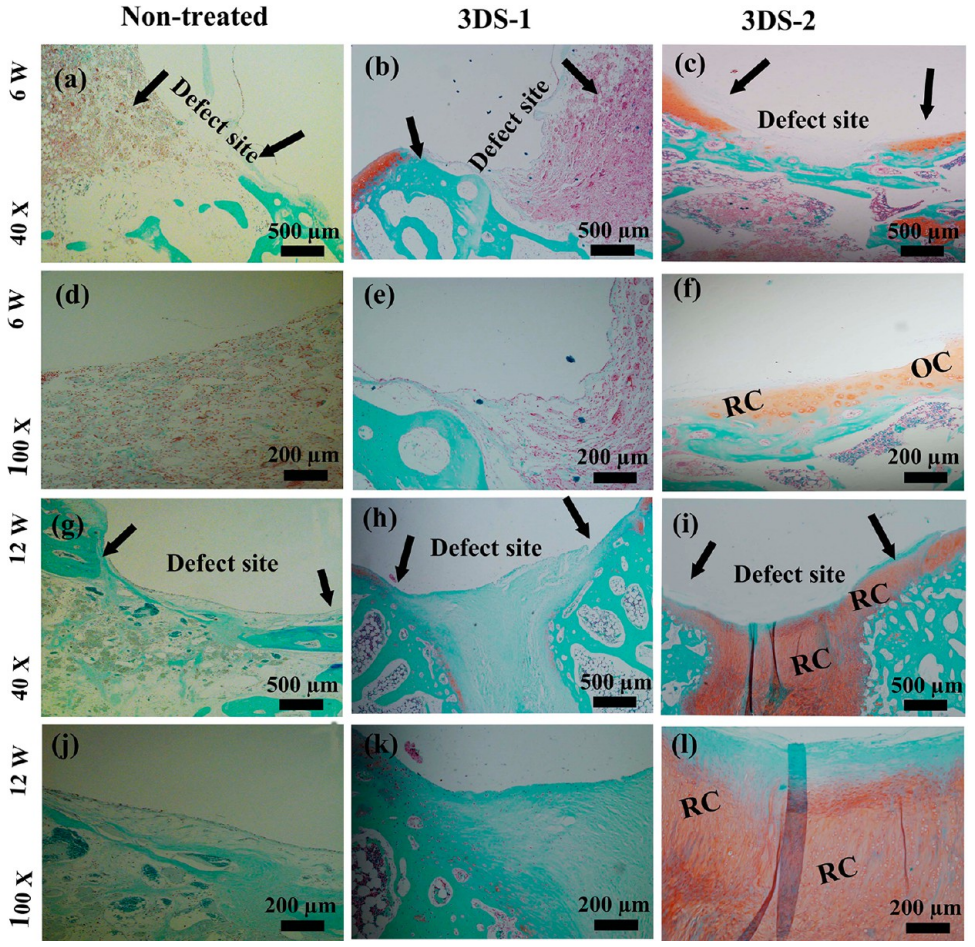

Figure 9. Histological analysis of cartilage defect area from three groups at 6 weeks (a–f) and 12 weeks (g–l) after surgery, stained with Safranin O-fast green. The defect was marked with black arrows in images (a–c, g–i). OC: original cartilage tissue. RC: repaired cartilage tissue.

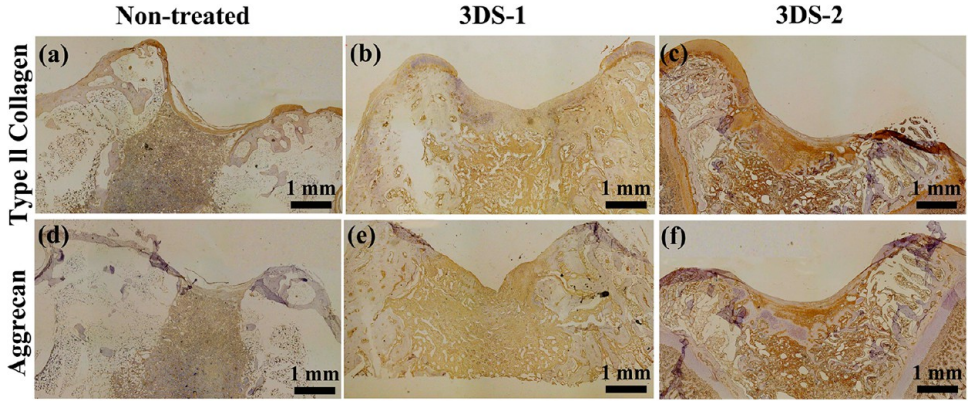

Figure 10. Immunohistochemical analysis of cartilage defect area from three groups at 12 weeks after surgery. Type collagen II immunohistochemical staining images (a–c) and aggrecan immunohistochemical staining images (d–f).

well integrated with original cartilage tissue (OC) which could be observed in Figure 7h. As shown in Figure 7e, Figure 7f, Figure 7h, and Figure 7i, cells were observed in the whole repaired area (3DS-1 and 3DS-2), and the defects in the 3DS-2 group were almost covered with regenerated cartilage tissue and chondrocytes.

For the nontreated group, at 6 weeks and 12 weeks after transplantation, only thin fibrous tissue in the joint surface of the defect could be observed as shown by H&E staining (Figure 8a, Figure 8d, Figure 8g, and Figure 8j)), and almost no staining (red) with Safranin O-fast green was observed (Figure 9a, Figure 9d, Figure 9g, and Figure 9j), indicating no GAG deposition. In the 3DS-1 group, at 6 weeks after transplantation, loose fibrous tissue was filled with the defect (Figure 8b and Figure 8e), and the fibrous tissue became more dense at 12 weeks (Figure 8h, Figure 8k, Figure 9h, and Figure 9k). No staining (red) with Safranin O-fast green in the defect was found at 6 weeks (Figure 9b and Figure 9e), but only a little staining (red) was observed at 12 weeks (Figure 9h). In the 3DS-2 group, a mixture of fibrous tissue and cartilage-like tissue

DOI: 10.1021/acsami.6b06825
ACS Appl. Mater. Interfaces 2016, 8, 24415–24425

was covered on the surface of defect at 6 weeks (Figure 8c and Figure 8f), and the staining with Safranin O-fast green showed a few GAG formed (Figure 9c and Figure 9f), indicting the partial cartilage formation. However, the defect was mainly repaired with thicker cartilage-like tissue at 12 weeks (Figure 8i and Figure 8l). Light staining (red) with Safranin O-fast green was observed (Figure 9i and Figure 9l) in the defect, which was similar to the normal surrounding cartilage tissue. In addition, immunohistochemical staining of the cartilage defect area showed that type collagen II and aggrecan deposition (brown color) were not strongly detected in the nontreated group (Figure. 10a and Figure 10d) and 3DS-1(Figure 10b and Figure 10e). However, intense type collagen II (Figure 10c) and aggrecan (Figure 10f) deposition were detected in 3DS-2, indicating the good production of ECM and the cartilage repair.

Duo to the limited capacity for self-repair of cartilage, it is still a clinical challenge for cartilage regeneration.[40] Cartilage tissue engineering provides a promising way to repair the damaged articular cartilage. In this present study, a nanofibrous scaffold (3DS-1) was prepared for cartilage regeneration. Figure 9 (h and k) showed little GAG formed after 3DS-1 was implanted in the defect for 12 weeks, and the results in vivo indicated that the repairing effect of 3DS-1 was limited. However, the 3DS-2 group showed thicker new cartilage and significant deposition of type collagen II and aggrecan, which indicated 3DS-2 would promote the regeneration and remodeling of the cartilage defect. HA is a native component of ECM in cartilage, which might the reason why the HA-based scaffold presents better repairing effect of cartilage.

4. CONCLUSION

In conclusion, two different 3D nanofibrous scaffolds were successfully fabricated. We explored a method to prepare 3DS-1 without using a toxic cross-linking agent. The mechanics of 3DS-1 could be enhanced by heat and water treatment. 3DS-1 possessed porous and nanofibrous structure, which could mimic the structure of natural ECM; in addition, it presented superabsorbent property and could improve the growth of chondrocytes in vitro. Compared with 3DS-1, 3DS-2 exhibited similar structure and water absorption property but higher compressive strength. Moreover, 3DS-2 could significantly repair the cartilage defect in rabbits. This nanofibrous scaffold might have potential for cartilage tissue engineering.

■ ASSOCIATED CONTENT

Supporting Information

The Supporting Information is available free of charge on the ACS Publications website at DOI: 10.1021/acsami.6b06825.

Optical photographs of wet scaffolds and the biodegradability of scaffolds (PDF)

■ AUTHOR INFORMATION

Corresponding Authors

*E-mail: xmm@dhu.edu.cn (Xiumei Mo).
*E-mail: fancunyi888@163.com (Cunyi Fan).

Author Contributions

#These authors contributed equally to this work.

Notes

The authors declare no competing financial interest.

■ ACKNOWLEDGMENTS

This study was supported by National Nature Science Foundation of China (31470941, 31271035), Science and Technology Commission of Shanghai Municipality (15JC1490100, 15441905100), The Fundamental Research Funds for the Central Universities (CUSF-DH-D-2016021), National Major Research Program of China (2016YFC1100200), PHD Programs Foundation of Ministry of Education of China (20130075110005), and light of textile project (J201404). The authors extend their appreciation to the International Scientific Partnership Program ISPP at King Saud University for its funding research through (ISPP-49).

■ REFERENCES

(1) Khorshidi, S.; Solouk, A.; Mirzadeh, H.; Mazinani, S.; Lagaron, J. M.; Sharifi, S.; Ramakrishna, S. A Review of Key Challenges of Electrospun Scaffolds for Tissue-Engineering Applications. *J. Tissue Eng. Regener. Med.* **2015**, 1−24.

(2) Cui, W.; Zhou, Y.; Chang, J. Electrospun Nanofibrous Materials for Tissue Engineering and Drug Delivery. *Sci. Technol. Adv. Mater.* **2010**, *11*, 14108−14118.

(3) Sill, T. J.; von Recum, H. A. Electrospinning: Applications in Drug Delivery and Tissue Engineering. *Biomaterials* **2008**, *29* (13), 1989−2006.

(4) Wang, X.; Ding, B.; Li, B. Biomimetic Electrospun Nanofibrous Structures for Tissue Engineering. *Mater. Today* **2013**, *16* (6), 229−241.

(5) Jiang, T.; Carbone, E. J.; Lo, W. H.; Laurencin, C. T. Electrospinning of Polymer Nanofibers for Tissue Regeneration. *Prog. Polym. Sci.* **2015**, *46*, 1−24.

(6) Shin, H. J.; Lee, C. H.; Cho, I. H.; Kim, Y.-J.; Lee, Y.-J.; Kim, I. A.; Park, K.-D.; Yui, N.; Shin, J.-W. Electrospun PLGA Nanofiber Scaffolds for Articular Cartilage Reconstruction: Mechanical Stability, Degradation and Cellular Responses under Mechanical Stimulation in Vitro. *J. Biomater. Sci., Polym. Ed.* **2006**, *17* (1−2), 103−119.

(7) Chen, J. P.; Su, C. H. Surface Modification of Electrospun PLLA Nanofibers by Plasma Treatment and Cationized Gelatin Immobilization for Cartilage Tissue Engineering. *Acta Biomater.* **2011**, *7* (1), 234−243.

(8) Shields, K. J.; Beckman, M. J.; Bowlin, G. L.; Wayne, J. S. Mechanical Properties and Cellular Proliferation of Electrospun Collagen Type II. *Tissue Eng.* **2004**, *10* (9−10), 1510−1517.

(9) Sun, B.; Long, Y. Z.; Zhang, H. D.; Li, M. M.; Duvail, J. L.; Jiang, X. Y.; Yin, H. L. Advances in Three-dimensional Nanofibrous Macrostructures via Electrospinning. *Prog. Polym. Sci.* **2014**, *39* (5), 862−890.

(10) Soliman, S.; Pagliari, S.; Rinaldi, A.; et al. Multiscale Three-Dimensional Scaffolds for Soft Tissue Engineering via Multimodal Electrospinning. *Acta Biomater.* **2010**, *6* (4), 1227−1237.

(11) Pham, Q. P.; Sharma, U.; Mikos, A. G. Electrospun Poly(ε-caprolactone) Microfiber and Multilayer Nanofiber/Microfiber Scaffolds: Characterization of Scaffolds and Measurement of Cellular Infiltration. *Biomacromolecules* **2006**, *7* (10), 2796−2805.

(12) Hong, S.; Kim, G. H. Fabrication of Size-Controlled Three-Dimensional Structures Consisting of Electrohydrodynamically Produced Polycaprolactone Micro/Nanofibers. *Appl. Phys. A: Mater. Sci. Process.* **2011**, *103* (4), 1009−1014.

(13) Wu, J.; Huang, C.; Liu, W.; Yin, A.; Chen, W.; He, C.; Wang, H.; Liu, S.; Fan, C.; Bowlin, G. L. Cell Infiltration and Vascularization in Porous Nanoyarn Scaffolds Prepared by Dynamic Liquid Electrospinning. *J. Biomed. Nanotechnol.* **2014**, *10* (4), 603−614.

(14) Badrossamay, M. R.; McIlwee, H. A.; Goss, J. A.; Parker, K. K. Nanofiber Assembly by Rotary Jet-Spinning. *Nano Lett.* **2010**, *10* (6), 2257−2261.

(15) Park, S. H.; Kim, T. G.; Kim, H. C.; Yang, D.-Y.; Park, T. G. Development of Dual Scale Scaffolds via Direct Polymer Melt

DOI: 10.1021/acsami.6b06825
ACS Appl. Mater. Interfaces 2016, 8, 24415−24425

Deposition and Electrospinning for Applications in Tissue Regeneration. *Acta Biomater.* **2008**, *4* (5), 1198−1207.
(16) Kim, T. G.; Chung, H. J.; Park, T. G. Macroporous and Nanofibrous Hyaluronic Acid/Collagen Hybrid Scaffold Fabricated by Concurrent Electrospinning and Deposition/Leaching of Salt Particles. *Acta Biomater.* **2008**, *4* (6), 1611−1619.
(17) Yan, G.; Yu, J.; Qiu, Y.; Yi, X.; Lu, J.; Zhou, X.; Bai, X. Self-Assembly of Electrospun Polymer Nanofibers: A General Phenomenon Generating Honeycomb-Patterned Nanofibrous Structures. *Langmuir* **2011**, *27* (8), 4285−4289.
(18) Ahirwal, D.; Hébraud, A.; Kádár, R.; Wilhelm, M.; Schlatter, G. From Self-Assembly of Electrospun Nanofibers to 3D cm Thick Hierarchical Foams. *Soft Matter* **2013**, *9* (11), 3164−3172.
(19) Nedjari, S.; Schlatter, G.; Hébraud, A. Thick Electrospun Honeycomb Scaffolds with Controlled Pore Size. *Mater. Lett.* **2015**, *142*, 180−183.
(20) Cai, Y. Z.; Zhang, G. R.; Wang, L. L.; Jiang, Y. Z.; Ouyang, H. W.; Zou, X. H. Novel Biodegradable Three-Dimensional Macroporous Scaffold Using Aligned Electrospun Nanofibrous Yarns for Bone Tissue Engineering. *J. Biomed. Mater. Res., Part A* **2012**, *100* (5), 1187−1194.
(21) Lavielle, N.; Hébraud, A.; Schlatter, G.; Thöny-Meyer, L.; Rossi, R. M.; Popa, A.-M. Simultaneous Electrospinning and Electrospraying: A Straightforward Approach for Fabricating Hierarchically Structured Composite Membranes. *ACS Appl. Mater. Interfaces* **2013**, *5* (20), 10090−10097.
(22) Wittmer, C. R.; Hébraud, A.; Nedjari, S.; Schlatter, G. Well-organized 3D Nanofibrous Composite Constructs Using Cooperative Effects Between Electrospinning and Electrospraying. *Polymer* **2014**, *55* (22), 5781−5787.
(23) Anderson, J. M.; Shive, M. S. Biodegradation and Biocompatibility of PLA and PLGA Microspheres. *Adv. Drug Delivery Rev.* **2012**, *64*, 72−82.
(24) Si, Y.; Fu, Q.; Wang, X.; Zhu, J.; Yu, J.; Sun, G.; Ding, B. Superelastic and Superhydrophobic Nanofiber-Assembled Cellular Aerogels for Effective Separation of Oil/Water Emulsions. *ACS Nano* **2015**, *9* (4), 3791−3799.
(25) Si, Y.; Yu, J.; Tang, X.; Ge, J.; Ding, B. Ultralight Nanofibre-Assembled Cellular Aerogels with Superelasticity and Multifunctionality. *Nat. Commun.* **2014**, *5*, 5802.
(26) Duan, G.; Jiang, S.; Jérôme, V.; Wendorff, J. H.; Fathi, A.; Uhm, J.; Altstädt, V.; Herling, M.; Breu, J.; Freitag, R.; Agarwal, Seema; Greiner, Andreas Ultralight, Soft Polymer Sponges by Self-Assembly of Short Electrospun Fibers in Colloidal Dispersions. *Adv. Funct. Mater.* **2015**, *25* (19), 2850−2856.
(27) Xu, T.; Miszuk, J. M.; Zhao, Y.; Sun, H.; Fong, H. Bone Tissue Engineering: Electrospun Polycaprolactone 3D Nanofibrous Scaffold with Interconnected and Hierarchically Structured Pores for Bone Tissue Engineering. *Adv. Healthcare Mater.* **2015**, *4* (15), 2237−2237.
(28) Chen, W.; Ma, J.; Zhu, L.; Morsi, Y.; Ei-Hamdshary, H.; Al-Deyab, S. S.; Mo, X. Superelastic, Superabsorbent and 3D Nanofiber-Assembled Scaffold for Tissue Engineering. *Colloids Surf., B* **2016**, *142*, 165−172.
(29) Panzavolta, S.; Gioffrè, M.; Focarete, M. L.; Gualandi, C.; Foroni, L.; Bigi, A. Electrospun Gelatin Nanofibers: Optimization of Genipin Cross-linking to Preserve Fiber Morphology after Exposure to Water. *Acta Biomater.* **2011**, *7* (4), 1702−1709.
(30) Mao, J. S.; Yin, Y. J.; De Yao, K. The Properties of Chitosan−Gelatin Membranes and Scaffolds Modified with Hyaluronic Acid by Different Methods. *Biomaterials* **2003**, *24* (9), 1621−1629.
(31) Jithendra, P.; Rajam, A. M.; Kalaivani, T.; Mandal, A. B.; Rose, C. Preparation and Characterization of Aloe Vera Blended Collagen-Chitosan Composite Scaffold for Tissue Engineering Applications. *ACS Appl. Mater. Interfaces* **2013**, *5* (15), 7291−7298.
(32) Zhang, S.; Chen, L.; Jiang, Y.; Cai, Y.; Xu, G.; Tong, T.; Zhang, W.; Wang, L.; Ji, J.; Shi, P. Bi-layer Collagen/Microporous Electrospun Nanofiber Scaffold Improves the Osteochondral Regeneration. *Acta Biomater.* **2013**, *9* (7), 7236−7247.
(33) Zhang, Y. Z.; Venugopal, J.; Huang, Z. M.; Lim, C. T.; Ramakrishna, S. Crosslinking of the Electrospun Gelatin Nanofibers. *Polymer* **2006**, *47* (8), 2911−2917.
(34) Yannas, I. V.; Tobolsky, A. V. Cross-linking of Gelatin by Dehydration. *Nature* **1967**, *215* (5100), 509−510.
(35) Silver, F. H.; Yannas, I. V.; Salzman, E. W. In Vitro Blood Compatibility of Glycosaminoglycan-Precipitated Collagens. *J. Biomed. Mater. Res.* **1979**, *13* (5), 701−716.
(36) Chang, K.-H.; Liao, H.-T.; Chen, J.-P. Preparation and Characterization of Gelatin/Hyaluronic Acid Cryogels for Adipose Tissue Engineering: in Vitro and in Vivo Studies. *Acta Biomater.* **2013**, *9* (11), 9012−9026.
(37) Zhang, F.; He, C.; Cao, L.; Feng, W.; Wang, H.; Mo, X.; Wang, J. Fabrication of Gelatin−Hyaluronic Acid Hybrid Scaffolds with Tunable Porous Structures for Soft Tissue Engineering. *Int. J. Biol. Macromol.* **2011**, *48* (3), 474−481.
(38) Arima, Y.; Iwata, H. Effect of Wettability and Surface Functional Groups on Protein Adsorption and Cell Adhesion Using Well-defined Mixed Self-Assembled Monolayers. *Biomaterials* **2007**, *28* (20), 3074−3082.
(39) Mankin, H. J.; Thrasher, A. Water Content and Binding in Normal and Osteoarthritic Human Cartilage. *J. Bone Joint Surg Am.* **1975**, *57* (1), 76−80.
(40) Yin, H.; Yu, W.; Zhen, S.; Xun, S.; Xu, Y.; Pan, L.; Meng, H.; Yu, X.; Bo, X.; Tian, F. Induction of Mesenchymal Stem Cell Chondrogenic Differentiation and Functional Cartilage Microtissue Formation for in Vivo Cartilage Regeneration by Cartilage Extracellular Matrix-Derived Particles. *Acta Biomater.* **2016**, *33*, 96−109.

DOI: 10.1021/acsami.6b06825
ACS Appl. Mater. Interfaces 2016, 8, 24415−24425